Influence of anharmonicity on the negative thermal expansion of α-Sn

Paweł T. Jochym,[1,*,†] Reinhard K. Kremer,[2,*,‡] Jan Łażewski,[1,*,§] Andrzej Ptok,[1] Przemysław Piekarz,[1] Eva Brücher,[2] and Andrzej M. Oleś[2,3]

[1]*Institute of Nuclear Physics, Polish Academy of Sciences, W. E. Radzikowskiego 152, PL-31342 Kraków, Poland*

[2]*Max Planck Institute for Solid State Research, Heisenbergstrasse 1, D-70569 Stuttgart, Germany*

[3]*Institute of Theoretical Physics, Jagiellonian University, Profesora Stanisława Łojasiewicza 11, PL-30348 Kraków, Poland*

(Received 9 April 2022; accepted 19 October 2022; published 2 November 2022)

The lattice vibrational properties of α-Sn (gray tin) were investigated experimentally by temperature-dependent x-ray diffraction and theoretically by density functional theory calculations. Similar to the other elements of group IV, α-Sn exhibits a lattice anomaly at low temperatures and negative thermal expansion, with a minimum at ∼27 K and a magnitude three times larger than in Si. The influence of anharmonic effects up to fourth-order potential terms on the phonon dispersion relations, the lattice parameters, and the thermal expansion coefficient have been tested. The performed analysis gives an excellent agreement with experiment when quartic potential terms are included in the theory. We point out that negative thermal expansion in α-Sn is not driven by the anharmonicity of the interatomic potential. This resolves the long-standing puzzle in the thermal behavior of α-Sn.

DOI: 10.1103/PhysRevMaterials.6.113601

I. INTRODUCTION

Recently, thin films of α-Sn grown epitaxially on InSb or CdTe substrates have been shown to host exotic topological phases. Their dimensionality can fortunately be tuned from three dimensional (3D) to two dimensional (2D) by varying the thickness and the strain of the films [1–5]. Related to these observations is the discovery of superconductivity below a few Kelvin in a stack of α-Sn ("stanene") layers deposited on PbTe/Bi_2Te_3/Si(111) substrates [6]. It was realized long ago that α-Sn is a promising system to investigate topological phases due to its large spin-orbit coupling [7,8]. From a more practical point of view, α-Sn offers a nontoxic alternative to other prime candidates for the realization of topological phases.

α-Sn, also known as "gray tin," as the lighter group-IV elements C (diamond), Si, and Ge crystallizes in the cubic, diamond-type structure (noncentrosymmetric space group $Fd\bar{3}m$, No. 227). It is stable at temperatures moderately below room temperature (∼286 K). The transformation from the metallic β-Sn ("elementary tin") into the cubic gray-to-black, brittle α-Sn modification, happens with an autocatalytic process which involves a substantial volume increase of ∼27% effecting the disintegration of the metallic β-Sn phase, a process colloquially known as "tin pest." α-Sn has a small-to-vanishing band gap, with the valence and conduction band touching each other at $\boldsymbol{k} = 0$ [7,9–14]. Sherrington and Kohn proposed that α-Sn may undergo an excitonic transition to a distorted phase at liquid-helium temperature lifting the band degeneracy, though strain fields or donor or acceptor impurities may inhibit it [15]. Halperin and Rice expected interesting many-body effects in the transport and other low-temperature properties of α-Sn [16].

Despite the increasing interest in the exotic low-temperature electronic phases, the knowledge of some elementary lattice properties of α-Sn remained rudimentary until today. The first characterizations of the lattice properties of α-Sn by optical spectroscopy techniques [17–20] were carried out about four decades ago on small single crystals grown using a mercury flux [21–23]. Noticeable lattice anharmonicity was concluded from the temperature dependence of first-order Raman scattering by phonons [24]. Other lattice properties such as, e.g., the vibrational specific-heat capacity down to liquid-helium temperatures remained fragmentary [25–28] [see the Supplemental Material (SM) [29]].

A lattice property closely related to phonon anharmonicity is the temperature dependence of the thermal expansion. At low temperatures, all isostructural group-IV elements, C (diamond), Si, and Ge, exhibit anomalies of their thermal expansion coefficient $\alpha(T)$. Whereas Si and Ge show negative thermal expansion (NTE) with minima at ∼83 K (Si) and ∼32 K (Ge) [30–34], $\alpha(T)$ of diamond remains positive, however, with a shallow minimum at ∼31 K [35]. Interestingly, binary systems crystallizing with the cubic zinc-blende crystal structure (closely related to the diamond-type structure), such as, e.g. the copper monohalides CuX (X = Cl, Br, I) also

*These authors contributed equally to this work.
†pawel.jochym@ifj.edu.pl
‡rekre@fkf.mpg.de
§jan.lazewski@ifj.edu.pl

Published by the American Physical Society under the terms of the Creative Commons Attribution 4.0 International license. Further distribution of this work must maintain attribution to the author(s) and the published article's title, journal citation, and DOI. Open access publication funded by the Max Planck Society.

exhibit NTE—for $X = \mathrm{Br}$ or I, however, only under sufficiently high pressures [36].

Qualitatively, NTE in semiconductors and insulators is often associated with the so-called *tension effect*, where transverse vibrations [37,38] leading to contraction must outweigh the volume increase with temperature (positive thermal expansion) due to the anharmonicity of the interatomic potential. Other mechanisms for NTE such as electronic or magnetostrictive effects or libration of linked polyhedra have also been discussed as a potential source of NTE [39–42]. The proximity to structural phase transitions can also give rise to NTE as recently has been observed, e.g., for SnSe [43]. The technological quest for thermal shock-resistant materials lately pushed the identification and characterization of a number of NTE ceramics, a prominent example being ZrW_2O_8 [44].

Ab initio calculations of the thermal expansion, including especially the low-temperature anomalous behavior, e.g., for Si, are a matter of ongoing debate. A quasiharmonic approximation (QHA), where harmonic phonons are adapted to the volume at a particular temperature, was employed to explain the NTE of Si at low temperatures [45,46]. However, recently it was argued by Kim *et al.* [47] that the success of the QHA is due to the cancellation of contributions of individual phonons and rather phonon anharmonicity and nuclear quantum effects have to be taken into account to understand the temperature dependence of the thermal expansion of Si. Here, by a combination of experiment and theory, we intend to compare the lattice properties of α-Sn with those of the other group-IV elements. Especially, the question is pertinent whether α-Sn will also exhibit NTE at low temperatures—and if so—how it can be modeled by first-principles calculations.

Early experiments by Novikova in 1961 on a compressed cylinder, in fact, indicated $\alpha(T)$ of α-Sn to become negative below 50 K [48]. However, these measurements carried out down to 25 K did not provide clear evidence for a minimum in $\alpha(T)$. Thewlis and Davey measured the lattice parameters of α-Sn between room temperature and 150 K and found a decrease with temperature, which corresponds to a constant linear thermal expansion coefficient of $\sim 5.5\times10^{-6}$ K^{-1} [49].

More recently, Souadkia *et al.* and Mehl *et al.* [50,51] investigated the lattice parameters and thermal expansion coefficient of α-Sn by density functional theory (DFT) calculations. Depending on the exchange-correlation energy functional used, they obtained values between $\sim 5\times10^{-6}$ and $\sim 7.5\times10^{-6}$ K^{-1} at room temperature [50,51], though their calculations using the Perdew-Burke-Ernzerhof (PBE) [52] generalized gradient approximation (GGA) tend to display a minimum of the lattice parameter at 40 K with the linear thermal expansion coefficient (α) approaching zero at 20 K [51]. The standard quasiharmonic calculations of Souadkia *et al.* [50] succeeded to reproduce the minimum in α at $\sim$30 K but did not offer any further analysis of the roots of this phenomenon. So far, no in-depth discussion was presented on the temperature dependence or mechanisms of the linear thermal expansion of α-Sn at very low temperatures.

In this paper we present the temperature dependence of the lattice parameters of α-Sn obtained by x-ray powder diffraction (XPD) measurements, from which we derive the thermal expansion coefficient $\alpha(T)$ between 12 and 280 K. Similarly to the other group-IV elements, our results show that α-Sn exhibits a lattice anomaly at low temperatures and negative thermal expansion with a minimum at 27 K and a magnitude three times larger than that of Si.

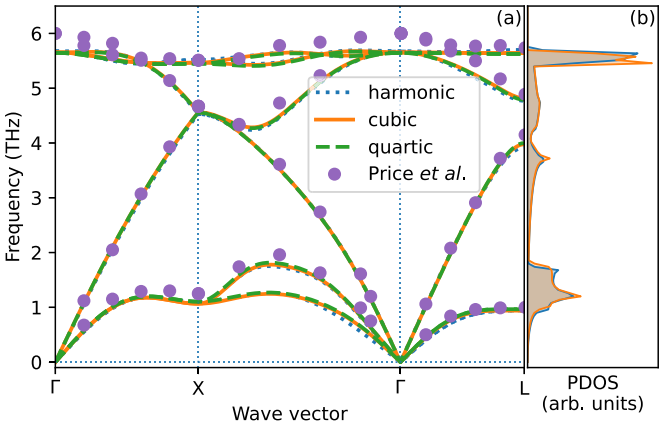

FIG. 1. (a) Phonon dispersion relations along the high-symmetry directions in the Brillouin zone obtained with and without anharmonic corrections, compared with measurements by Price *et al.* [60]. (b) The PDOS derived from harmonic (blue) and quartic (orange) approximation—they are plotted together to show differences arising by the inclusion of anharmonic effects.

II. DFT CALCULATIONS

In our DFT calculations of the phonon dispersion relations, the lattice parameters and the thermal expansion coefficient the anharmonic effects up to fourth-order potential terms have been included. Figure 1 shows excellent agreement between calculated phonon dispersions and neutron measurements. A detailed analysis of the lattice properties of α-Sn reveals that taking anharmonicity of the vibrational potentials into account is crucial to quantitatively understand the experimental results. We found that anharmonic corrections bring a significant improvement to a harmonic potential description, which grossly fails to reproduce the experimental results at higher temperatures. In addition to the temperature dependence of the lattice parameter and thermal expansion, we also checked our theoretical predictions against specific-heat measurements carried out over the whole temperature range from room temperature down to liquid-helium temperature.

The DFT calculations were performed for a $2\times2\times2$ supercell containing 64 Sn atoms using the projector augmented-wave potentials [53] implemented in the VASP code [54]. A $4\times4\times4$ **k**-point grid was used for the reciprocal space sampling. Additionally, the convergence of the lattice parameter and phonon dispersion relations was verified for a denser mesh of $8\times8\times8$. The plane-wave basis set was reduced by setting the energy cutoff to 150 eV.

III. QUASIHARMONIC APPROXIMATION WITH ANHARMONIC CORRECTIONS

To include anharmonic effects, the system was characterized by statistical ensembles of potential energy distribution corresponding to a number of selected temperatures T_b [55].

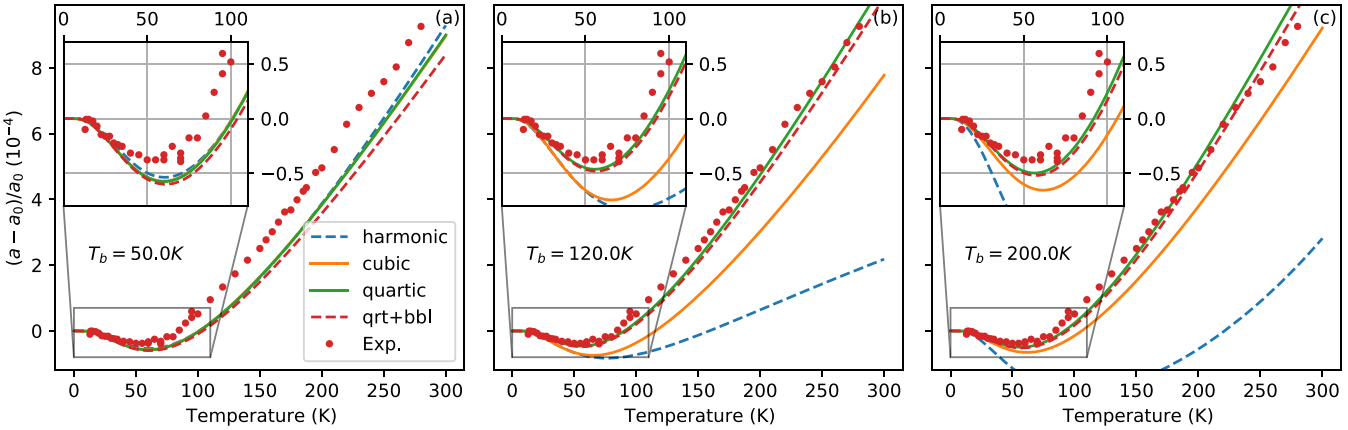

FIG. 2. Lattice parameter of α-Sn obtained from the x-ray diffraction between 12 and 280 K. Theoretical results obtained within quasiharmonic approximation including the harmonic (blue dashed line), cubic (orange line), quartic (green line), and bubble (red dashed line) corrections to free energy and using base temperatures $T_b = 50$, 120, and 200 K [(a)–(c), respectively; see description in text].

A high-efficiency configuration space sampling (HECSS) method [56] was employed to generate, for each considered system and T_b temperature, 40 different configurations of atomic displacements in the supercell. The interatomic force constants were obtained with the ALAMODE software [57], using the supercell technique. Calculations were performed for the thermal distributions of multidisplacement of atoms for given finite temperatures [55], generated within the HECSS procedure [56]. In the calculations, we included both harmonic and higher-order contributions to the potential energy. The calculated frequencies were always derived from the quadratic term in the energy surface expansion. The influence of higher-energy terms was checked by including bubble-diagram corrections to the free energy [58]. Their influence on the thermal expansion curves proved to be negligible (see Fig. 2). No further anharmonic effects (e.g., frequency shift, peak broadening) were included in our calculations.

We used three different exchange-correlation energy functionals: (i) the local density approximation (LDA), (ii) GGA in PBE parametrization [52], and (iii) the nonempirical strongly constrained and appropriately normed (SCAN) meta-GGA functional [59]. Within these approximations, we obtained the following values for the cubic lattice parameter a: 6.4785 Å (LDA), 6.6523 Å (PBE), and 6.5564 Å (SCAN). As in the previous calculations [51], the LDA result shows the best agreement with the experimental value for the lattice parameter (6.484 Å), while the PBE and SCAN functionals overestimate it.

Figure 1 displays the phonon dispersion relations and the phonon density of states (PDOS) obtained with and without including anharmonicity up to fourth order in comparison with the experimental data measured by Price *et al.* [60]. The phonon dispersion relations calculated within the LDA approximation agree very well with the neutron measurements taken at 90 K [see Fig. 1(a)] and with previous calculations [28,61,62], whereas the results obtained for the PBE correlation functional underestimate the experimental data (see Sec. SI in the SM [29]). Anharmonicity effects on the phonon dispersion relations are small and affect primarily the acoustic phonon branches and some optical phonons [see Fig. 1(a)].

As it has been similarly observed for Si and Ge [63], a salient characteristic of the transverse acoustic phonons of α-Sn is that their dispersion becomes relatively flat on approaching the boundaries of the Brillouin zone and that their energies are much lower than those of the longitudinal acoustic phonons. As a consequence, the PDOS of α-Sn is characterized by two main features: a broader ridge between 0.9 and 1.7 THz with a spike at 1.2 THz arising from the acoustic phonons with low dispersion along the Γ-X and the Γ-L direction in the Brillouin zone. Optical phonons generate two very sharp spikes in the PDOS between 5.5 and 5.7 THz. As can be seen in Fig. 1(b), including anharmonicity effects enhances the peak in the PDOS at 1.2 THz and especially the sharp spike originating from the optical phonons at 5.5 THz. The PDOS including anharmonicity was used to calculate the specific heat of α-Sn. In Fig. S1 in the SM [29] we compare the results of our specific-heat measurements carried out between 2 and 280 K with preceding results and the calculations. Experiment and theory agree well. Especially the position of the prominent peak in the C_p/T^3 representation is well reproduced, though the magnitude of the calculated maximum is somewhat higher.

The lattice parameters of a polycrystalline sample of α-Sn between 12 and 280 K obtained by Rietveld refinements [64] of the XPD patterns measured at stabilized temperatures are displayed in Fig. 2 together with our theoretical results (for more experimental details, see Fig. S2 in the SM [29]). With growing temperature the lattice parameter decreases and reaches a minimum at $T = 52$ K and finally increases linearly above 150 K. The theoretical lattice parameter obtained within the QHA shows a similar qualitative behavior, however, the observed decrease of the lattice parameter at low temperatures is stronger than that obtained from experiment and the minimum is found at ∼70 K.

Including anharmonic potential corrections leads to an improved quantitative agreement between theory and experiment. The theoretical lines plotted in Fig. 2 are obtained with the modified QHA procedure based on phonon

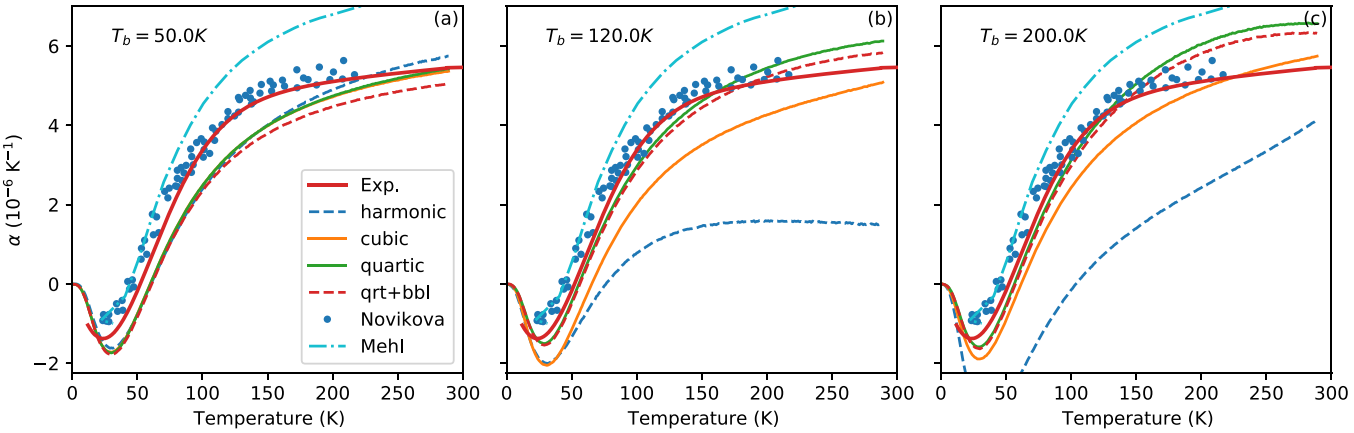

FIG. 3. Thermal expansion of α-Sn. Our experimental data calculated from the Padé approximation (see the Supplemental Material) are shown by the red line. Theoretical results obtained with the harmonic (blue dashed line), cubic (orange line), quartic (green line), and bubble (red dashed line) corrections and using base temperatures $T_b = 50$, 120, and 200 K [(a)–(c), respectively; see description in text]. The cyan dashed-dotted line represents the data by Mehl *et al.* [51] and the data by Novikova are marked with blue dots [48].

frequencies derived from the harmonic term in the quadratic, cubic, and quartic fits to the potential energy surface. The three panels correspond to the selected temperatures T_b of the thermodynamic ensemble used in the interatomic interactions modeling with HECSS procedure [56] (see Sec. SII in the SM [29] for further details). Higher temperatures T_b correspond to a larger energy range sampled by the considered thermodynamic ensemble. For $T_b = 50$ K, the three fits give very similar results in a wide range of temperatures and agree fairly well with the experimental data points at the lowest temperatures, demonstrating that anharmonic effects are not essential, and the harmonic approximation already provides a good description of the volume contraction. For larger values of T_b, the harmonic approximation strongly differs from the experimental data and shows much stronger NTE. The agreement of experiment and theory improves if cubic potential terms are also considered in the potential energy. Best agreement, especially for $T_b = 120$ K, is achieved by including quartic potential terms.

IV. THERMAL EXPANSION COEFFICIENT

The thermal expansion coefficient (TEC) of α-Sn as a function of temperature, displayed in Fig. 3, was obtained from the numerical derivative of a Padé approximant of the lattice parameters (for more details, see the SM [29]). We observe a negative TEC below 52 K and a minimum of $\alpha(T)$ at $\sim$27 K with a value of 1.35×10^{-6} K. At higher temperatures our data agree well with Novikova's results if their temperature scale is upshifted by $\sim$7 K. Towards room temperature we obtain a linear TEC of about $\sim5\times10^{-6}$ K^{-1}, in stark disagreement with the results obtained recently by Mehl *et al.* from the quasiharmonic GGA calculations [51].

From our calculations one can conclude that the harmonic term of the potential is crucial and already sufficient to reproduce the NTE of α-Sn and quantitatively to a good approximation explains it by the frequency shifts captured by the quasiharmonic approximation. The small difference between the harmonic part of the fourth-order model with a quartic term (green line) and anharmonic model including phonon-phonon interactions (bubble term, red dashed line in Fig. 3) clearly demonstrates that bubble-diagram anharmonic corrections to the vibrational free energy (i.e., frequency shifts due to the nonquadratic shape of the interatomic potential) have a negligible effect on the thermal expansion of α-Sn. This observation is consistent with negligible frequency shifts depicted in Fig. 1.

However, our results simultaneously show that the potential is substantially anharmonic in the temperature range above $T_b \approx 50$ K, consistent with early Raman scattering experiments [24]. There, it cannot be successfully modeled with a simple quadratic fit (blue dashed line). The role of anharmonic terms in the potential is further illustrated by Fig. S2 in Sec. SII of the SM [29]. We suspect that the GGA quasiharmonic model proposed by Mehl *et al.* [51] also fails partially for the same reason. Note that even cubic corrections do not allow matching the experiment properly (orange line in the same figure).

For Si it has been shown that the low-energy transverse acoustic phonons exhibit pronounced negative mode Grüneisen parameters [65]. To investigate the role of low-energy transverse acoustic phonons in NTE, we calculated the mode Grüneisen parameters for the acoustic and optic phonons of α-Sn. We find that the Grüneisen parameters for all transverse acoustic modes are negative, e.g., at the X point in the Brillouin zone by about a factor of three larger in magnitude than for Si (see Fig. S6 in Sec. SVI in the SM [29]). This finding emphasizes the crucial role of these phonons in NTE observed in α-Sn and also allows to understand the markedly increased NTE of α-Sn as compared to Si.

V. CONCLUSIONS

In summary, we have demonstrated that α-Sn exhibits negative thermal expansion below 50 K. Our measurements, extending the previous temperature range for the α-Sn down to 12 K, show a clear minimum of the linear thermal expansion coefficient at 27 K. The magnitude of the negative

expansion anomaly is by factor of three larger than that of Si. By first-principles calculations, we have found that the negative thermal expansion can be qualitatively modeled within the quasiharmonic approximation using only the harmonic part of the potential.

Additionally, we have shown the marginal role of the fourth-order corrections to the vibrational free energy of the material. Thus, negative thermal expansion in α-Sn is *de facto* not driven by the anharmonicity of the interatomic potential, but it can be already understood on the basis of harmonic frequency shifts captured by the quasiharmonic approximation. However, to *quantitatively* reproduce the thermal expansion up to room temperature, the higher-order anharmonic terms must be included in the modeling of the interatomic interactions, which properly captures the changes in vibrational frequencies in the material.

ACKNOWLEDGMENTS

P.P. acknowledges the support by Narodowe Centrum Nauki (NCN, National Science Centre, Poland), under Project No. 2017/25/B/ST3/02586. A.P. appreciates funding in the frame of scholarships of the Minister of Science and Higher Education (Poland) for outstanding young scientists (No. 818/STYP/14/2019). A.M.O. is grateful for support via the Alexander von Humboldt Foundation Fellowship [66] (Humboldt-Forschungspreis).

[1] L. Fu and C. L. Kane, Topological insulators with inversion symmetry, Phys. Rev. B **76**, 045302 (2007).

[2] A. Barfuss, L. Dudy, M. R. Scholz, H. Roth, P. Höpfner, C. Blumenstein, G. Landolt, J. H. Dil, N. C. Plumb, M. Radovic, A. Bostwick, E. Rotenberg, A. Fleszar, G. Bihlmayer, D. Wortmann, G. Li, W. Hanke, R. Claessen, and J. Schäfer, Elemental Topological Insulator with Tunable Fermi Level: Strained α-Sn On InSb(001), Phys. Rev. Lett. **111**, 157205 (2013).

[3] S. Küfner, M. Fitzner, and F. Bechstedt, Topological α-Sn surface states versus film thickness and strain, Phys. Rev. B **90**, 125312 (2014).

[4] H. Huang and F. Liu, Tensile strained gray tin: Dirac semimetal for observing negative magnetoresistance with Shubnikov–de Haas oscillations, Phys. Rev. B **95**, 201101(R) (2017).

[5] C.-Z. Xu, Y.-H. Chan, Y. Chen, P. Chen, X. Wang, C. Dejoie, M.-H. Wong, J. A. Hlevyack, H. Ryu, H.-Y. Kee, N. Tamura, M.-Y. Chou, Z. Hussain, S.-K. Mo, and T.-C. Chiang, Elemental Topological Dirac Semimetal: α-Sn On InSb(111), Phys. Rev. Lett. **118**, 146402 (2017).

[6] M. Liao, Y. Zang, Z. Guan, H. Li, Y. Gong, K. Zhu, X.-P. Hu, D. Zhang, Y. Xu, Y.-Y. Wang, K. He, X.-C. Ma, S.-C. Zhang, and Q.-K. Xue, Superconductivity in few-layer stanene, Nat. Phys. **14**, 344 (2018).

[7] F. Bassani and L. Liu, Electronic band structure of gray tin, Phys. Rev. **132**, 2047 (1963).

[8] *Intrinsic Properties of Group IV Elements and III-V, II-VI and I-VII Compounds*, edited by O. Madelung, W. von der Osten, and U. Rössler, Landolt-Börnstein, New Series, Group III, Vol. 22, Pt. A (Springer, Berlin, 1987), pp. 39–43.

[9] G. Busch, J. Wieland, and H. Zoller, Versuche zur Messung der elektrischen Leitfähigkeit des grauen Zinns, Helv. Phys. Acta **23**, 528 (1950).

[10] A. W. Ewald and E. E. Kohnke, Measurements of electrical conductivity and magnetoresistance of gray tin filaments, Phys. Rev. **97**, 607 (1955).

[11] S. Groves and W. Paul, Band Structure of Gray Tin, Phys. Rev. Lett. **11**, 194 (1963).

[12] F. Herman, Speculations on the energy band structure of zinc-blende-type crystals, Int. J. Electron. **1**, 103 (1955).

[13] A. Continenza and A. J. Freeman, Structural and electronic properties of α-Sn, CdTe, and their [001] monolayer superlattices, Phys. Rev. B **43**, 8951 (1991).

[14] R. A. Carrasco, C. M. Zamarripa, S. Zollner, J. Menéndez, S. A. Chastang, J. Duan, G. J. Grzybowski, B. B. Claflin, and A. M. Kiefer, The direct bandgap of gray α-tin investigated by infrared ellipsometry, Appl. Phys. Lett. **113**, 232104 (2018).

[15] D. Sherrington and W. Kohn, Speculations about grey tin, Rev. Mod. Phys. **40**, 767 (1968).

[16] B. I. Halperin and T. M. Rice, Possible anomalies at a semimetal–semiconductor transition, Rev. Mod. Phys. **40**, 755 (1968).

[17] M. Cardona, R. K. Kremer, M. Sanati, S. K. Estreicher, and T. R. Anthony, Measurements of the heat capacity of diamond with different isotopic compositions, Solid State Commun. **133**, 465 (2005).

[18] M. Cardona, K. L. Shaklee, and F. H. Pollak, Electroreflectance at a semiconductor-electrolyte interface, Phys. Rev. **154**, 696 (1967).

[19] C. J. Buchenauer, M. Cardona, and F. H. Pollak, Raman scattering in gray tin, Phys. Rev. B **3**, 1243 (1971).

[20] M. Iliev, M. Sinyukov, and M. Cardona, Resonant first- and second-order raman scattering in gray tin, Phys. Rev. B **16**, 5350 (1977).

[21] A. W. Ewald and O. N. Tufte, Gray tin single crystals, J. Appl. Phys. **29**, 1007 (1958).

[22] P. Van Lent, The preparation of gray tin single crystals by transformation of tin-mercury alloys, Acta Metall. **10**, 1089 (1962).

[23] S. H. Groves, C. R. Pidgeon, A. W. Ewald, and R. J. Wagner, Interband magnetoreflection of α-Sn, J. Phys. Chem. Solids **31**, 2031 (1970).

[24] J. Menéndez and M. Cardona, Temperature-dependence of the first-order Raman scattering by phonons in Si, Ge, and α-Sn: Anharmonic effects, Phys. Rev. B **29**, 2051 (1984).

[25] F. Lange, Untersuchungen über die spezifische Wärme bei tiefen Temperaturen, Z. Phys. Chem. **110U**, 343 (1924).

[26] R. W. Hill and D. H. Parkinson, XXV. The specific heats of germanium and grey tin at low temperatures, Philos. Mag. **43**, 309 (1952).

[27] F. J. Webb, J. Wilks, and F. E. Simon, The measurement of lattice specific heats at low temperatures using a heat switch, Proc. R. Soc. London, Ser. A **230**, 549 (1955).

[28] S.-H. Na and C.-H. Park, First-principles study of structural phase transition of Sn, J. Korean Phys. Soc. **56**, 494 (2010).

[29] See Supplemental Material at http://link.aps.org/supplemental/10.1103/PhysRevMaterials.6.113601 for the phonon dispersions obtained within the GGA, extended QHA procedure, the experimental details, the heat capacity measurements, and the Grüneisen parameter calculations.
[30] H. Ibach, Thermal expansion of silicon and zinc oxide (I), Phys. Status Solidi B **31**, 625 (1969).
[31] K. G. Lyon, G. L. Salinger, C. A. Swenson, and G. K. White, Linear thermal expansion measurements on silicon from 6 to 340 K, J. Appl. Phys. **48**, 865 (1977).
[32] G. A. Slack and S. F. Bartram, Thermal expansion of some diamondlike crystals, J. Appl. Phys. **46**, 89 (1975).
[33] P. W. Sparks and C. A. Swenson, Thermal expansions from 2 to 40° K of Ge, Si, and four III-V compounds, Phys. Rev. **163**, 779 (1967).
[34] R. R. Reeber and K. Wang, Thermal expansion and lattice parameters of group IV semiconductors, Mater. Chem. Phys. **46**, 259 (1996).
[35] S. Stoupin and Y. V. Shvyd'ko, Thermal Expansion of Diamond at Low Temperatures, Phys. Rev. Lett. **104**, 085901 (2010).
[36] A. M. Gopakumar, M. K. Gupta, R. Mittal, S. Rols, and S. L. Chaplot, Investigating anomalous thermal expansion of copper halides by inelastic neutron scattering and ab initio phonon calculations, Phys. Chem. Chem. Phys. **19**, 12107 (2017).
[37] T. H. K. Barron, Grüneisen parameters for the equation of state of solids, Ann. Phys. **1**, 77 (1957).
[38] T. H. K. Barron, J. G. Collins, and G. K. White, Thermal-expansion of solids at low-temperatures, Adv. Phys. **29**, 609 (1980).
[39] M. T. Dove and H. Fang, Negative thermal expansion and associated anomalous physical properties: Review of the lattice dynamics theoretical foundation, Rep. Prog. Phys. **79**, 066503 (2016).
[40] J. P. Attfield, Mechanisms and materials for NTE, Front. Chem. **6**, 371 (2018).
[41] R. Mittal, M. K. Gupta, and S. L. Chaplot, Phonons and anomalous thermal expansion behaviour in crystalline solids, Prog. Mater. Sci. **92**, 360 (2018).
[42] N. Z. Koocher, L.-F. Huang, and J. M. Rondinelli, Negative thermal expansion in the Ruddlesden-Popper calcium titanates, Phys. Rev. Mater. **5**, 053601 (2021).
[43] D. Bansal, J. Hong, C. W. Li, A. F. May, W. Porter, M. Y. Hu, D. L. Abernathy, and O. Delaire, Phonon anharmonicity and negative thermal expansion in SnSe, Phys. Rev. B **94**, 054307 (2016).
[44] T. A. Mary, J. S. O. Evans, T. Vogt, and A. W. Sleight, Negative thermal expansion from 0.34 to 1050 Kelvin in ZrW_2O_8, Science **272**, 90 (1996).
[45] B. Fultz, Vibrational thermodynamics of materials, Prog. Mater. Sci. **55**, 247 (2010).
[46] E. T. Ritz, S. J. Li, and N. A. Benedek, Thermal expansion in insulating solids from first principles, J. Appl. Phys. **126**, 171102 (2019).
[47] D. S. Kim, O. Hellman, J. Herriman, H. L. Smith, J. Y. Y. Lin, N. Shulumba, J. L. Niedziela, C. W. Li, D. L. Abernathy, and B. Fultz, Nuclear quantum effect with pure anharmonicity and the anomalous thermal expansion of silicon, Proc. Natl. Acad. Sci. USA **115**, 1992 (2018).
[48] S. I. Novikova, Study of the thermal expansion of alpha-Sn, InSb, and CdTe, Sov. Phys. Solid State **2**, 2087 (1981) [Fiz. Tverd. Tela (Leningrad) **2**, 2341 (1960)].
[49] J. Thewlis and A. R. Davey, Thermal expansion of grey tin, Nature (London) **174**, 1011 (1954).
[50] M. Souadkia, B. Bennecer, and F. Kalarasse, Elastic, vibrational and thermodynamic properties of based group IV semiconductors and GeC under pressure, J. Phys. Chem. Solids **74**, 1615 (2013).
[51] M. J. Mehl, M. Ronquillo, D. Hicks, M. Esters, C. Oses, R. Friedrich, A. Smolyanyuk, E. Gossett, D. Finkenstadt, and S. Curtarolo, Tin-pest problem as a test of density functionals using high-throughput calculations, Phys. Rev. Mater. **5**, 083608 (2021).
[52] J. P. Perdew, K. Burke, and M. Ernzerhof, Generalized Gradient Approximation Made Simple, Phys. Rev. Lett. **77**, 3865 (1996).
[53] P. E. Blöchl, Projector augmented-wave method, Phys. Rev. B **50**, 17953 (1994).
[54] G. Kresse and J. Hafner, *Ab initio* molecular-dynamics simulation of the liquid-metal–amorphous-semiconductor transition in germanium, Phys. Rev. B **49**, 14251 (1994).
[55] O. Hellman, I. A. Abrikosov, and S. I. Simak, Lattice dynamics of anharmonic solids from first principles, Phys. Rev. B **84**, 180301(R) (2011).
[56] P. T. Jochym and J. Łażewski, High efficiency configuration space sampling–probing the distribution of available states, SciPost Phys. **10**, 129 (2021).
[57] T. Tadano, Y. Gohda, and S. Tsuneyuki, Anharmonic force constants extracted from first-principles molecular dynamics: applications to heat transfer simulations, J. Phys.: Condens. Matter **26**, 225402 (2014).
[58] Y. Oba, T. Tadano, R. Akashi, and S. Tsuneyuki, First-principles study of phonon anharmonicity and negative thermal expansion in ScF_3, Phys. Rev. Mater. **3**, 033601 (2019).
[59] J. Sun, A. Ruzsinszky, and J. P. Perdew, Strongly Constrained and Appropriately Normed Semilocal Density Functional, Phys. Rev. Lett. **115**, 036402 (2015).
[60] D. L. Price, J. M. Rowe, and R. M. Nicklow, Lattice dynamics of grey tin and indium antimonide, Phys. Rev. B **3**, 1268 (1971).
[61] W. Weber, Adiabatic bond charge model for the phonons in diamond, Si, Ge, and α-Sn, Phys. Rev. B **15**, 4789 (1977).
[62] P. Pavone, S. Baroni, and S. de Gironcoli, $\alpha \leftrightarrow \beta$ phase transition in tin: A theoretical study based on density-functional perturbation theory, Phys. Rev. B **57**, 10421 (1998).
[63] P. Yu and M. Cardona, *Fundamentals of Semiconductors: Physics and Materials Properties* (Springer, Berlin, 2010).
[64] J. Rodríguez-Carvajal, Recent advances in magnetic structure determination by neutron powder diffraction, Phys. B: Condens. Matter **192**, 55 (1993).
[65] C. H. Xu, C. Z. Wang, C. T. Chan, and K. M. Ho, Theory of the thermal expansion of Si and diamond, Phys. Rev. B **43**, 5024 (1991).
[66] https://www.humboldt-foundation.de/web/humboldt-preis.html.